Rapid Communications

Quantitative subcompound-mediated reaction model for the molecular beam epitaxy of III-VI and IV-VI thin films: Applied to Ga_2O_3, In_2O_3, and SnO_2

Patrick Vogt* and Oliver Bierwagen

Paul-Drude-Institut für Festkörperelektronik, Leibniz-Institut im Forschungsverbund Berlin e.V., Hausvogteiplatz 5–7, 10117 Berlin, Germany

(Received 14 November 2017; published 20 December 2018; corrected 9 July 2020)

We identify a novel reaction mechanism in the thin film synthesis of compound materials. With the example of the O plasma-assisted molecular beam epitaxy of III-O and IV-O semiconductors—Ga_2O_3, In_2O_3, and SnO_2—we illustrate this mechanism, involving the intermediate formation of a suboxide. This consecutive reaction mechanism, as well as the competing desorption of a subcompound, are the basis for the development of a quantitative growth model parametrized by three material-dependent parameters. It is proposed and justified to be applicable to other III-VI and IV-VI compounds whose constituents exhibit analogous kinetic and thermodynamic properties to those discussed for oxides. We validate this model quantitatively by experimental growth rate and desorption data as a function of all growth parameters for Ga_2O_3, In_2O_3, and SnO_2. As the first of its kind, our model serves as a basis for more sophisticated growth models, e.g., describing multicomponent materials or including surface diffusion processes, and can be transferred to other growth techniques and thin films that grow via intermediate reaction products.

DOI: 10.1103/PhysRevMaterials.2.120401

The epitaxy of semiconductors enabled the advent of solid-state electronics, with applications for telecommunication and solid-state lighting [1,2], governing our modern daily life. The heterostructures used in these applications can be synthesized by molecular beam epitaxy (MBE) at highest crystal quality. Thus MBE is a key technique for thin film growth, allowing the study of fundamental crystal properties [3–5], and likewise facilitates the study of elemental reaction mechanisms in a growing thin film [6].

The MBE of III-V and II-VI semiconductors is rather simple: they form via a single-step reaction process where monoatomic cations react with monoatomic anions directly to the III-V [7,8] or II-VI compound [9,10]. In the case of a V-rich or VI-rich flux ratio, this basic reaction mechanism warrants group III or group II atoms, respectively, to be fully incorporated—such as for the MBE of III-P, III-As, III-Sb, III-N, or II-O materials [6–9,11]. III-N films, however, are typically grown in the group III-rich regime to obtain the highest crystalline and morphological quality [12–14]. Here, the growth rate Γ is independent on the III/N flux ratio [8,15].

III-VI and IV-VI compounds, such as Ga_2O_3, In_2O_3, and SnO_2, are semiconductors with physical properties desired for future applications. They posses high tunable electrical conductivity, and based on their wide band gaps, they have a high potential for the next generation of optoelectronic applications and high-power electronic devices [16–18].

The MBE of these metal (Me) oxides has been investigated qualitatively. Their Γ in the Me-rich regimes is strongly influenced by the Me-to-O flux ratios $R = \phi_{Me}/\phi_O$ [19–23], with Me fluxes and O fluxes denoted as ϕ_{Me} and ϕ_O, respectively. In addition, Γ is highly dependent on the growth temperature T_G [22,23]. The reason for these dependencies is the formation and desorption of volatile suboxides [19–23].

The aim of achieving high-quality III-O and IV-O layers controlled by growth conditions necessitates a quantitative understanding on their growth mechanisms, similar to that of III-V and II-VI semiconductors. To date, however, such a quantitative and comprehensive understanding on the reaction behavior of III-VI and IV-VI semiconductors is lacking.

In this Rapid Communication, we identify the microscopic reaction mechanism of III-O and IV-O compounds as a two-step reaction process. This mechanism includes the intermediate oxidation of a Me to a suboxide, followed by a further oxidation of a suboxide to a solid Me oxide compound, or by a competing suboxide desorption. We quantitatively present the O plasma-assisted MBE (PAMBE) of these classes of materials by a reaction-rate based Γ model and present their complete reaction scheme. Our model explicitly describes all experimental results on Ga_2O_3, In_2O_3, and SnO_2. Our findings presented here are fundamentally different from the single-step III-V and II-VI MBE, and we propose them to be valid for the MBE of various III-VI and IV-VI thin films.

Our model and findings derived below (mainly) use our published Γ [measured by laser reflectometry (LR)], and respective desorption γ data [measured by line-of-sight quadrupole mass spectrometry (QMS)], of Ga_2O_3 [21,22], In_2O_3 [23], and SnO_2 [21]. Thus we want to review here their Γ evolutions depending on ϕ_{Me}, ϕ_O, and T_G, briefly; Figs. 1 and 2 plot Γ of Ga_2O_3 as well as In_2O_3 and SnO_2 as a function of ϕ_{Me} (Me = Ga, In, Sn) and T_G, respectively. At low T_G, Γ increases linearly with ϕ_{Me} in the O-rich regimes (gray areas in data panels) for all $R = \phi_{Me}/\phi_O \leqslant x/y$. The stoichiometric coefficients of cations and anions in Me_2O_3 and SnO_2 are $x = 2$ and $y = 3$ as well as $x = 1$ and $y = 2$, respectively. Once the Me-rich regimes (white areas in data panels) are entered, i.e., for $R > x/y$, Γ decreases linearly with ϕ_{Me} because of

*vogt@pdi-berlin.de

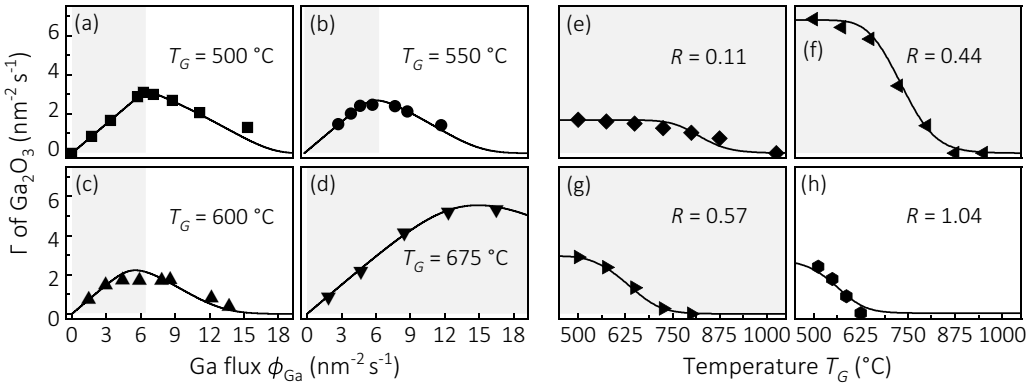

FIG. 1. (a)–(d) and (e)–(h) Dependence of Γ for Ga_2O_3 on ϕ_{Ga} at different $T_G \pm 15$ °C, and on T_G at different $R \pm 0.02$, respectively. Corresponding parameters are indicated in the figures. Symbols represent experimental data and solid lines are model predictions by Eqs. (8), (10), and (11). In (a), (b), (c), (g), (h) and in (d), (e), (f) ϕ_O was 10.2 and 30.6 nm^{-2} s^{-1}, respectively.

the O-deficiency-induced desorption of a suboxide Me_xO_{y-x}; and ceases completely at $R = x$ [21]. As a function of T_G, Γ decreases monotonically for all R as caused by additionally thermally activated Me_xO_{y-x} desorption. This decrease is more pronounced at higher R [22,23]. We note, we have never observed Me desorption for all compounds investigated and growth conditions employed.

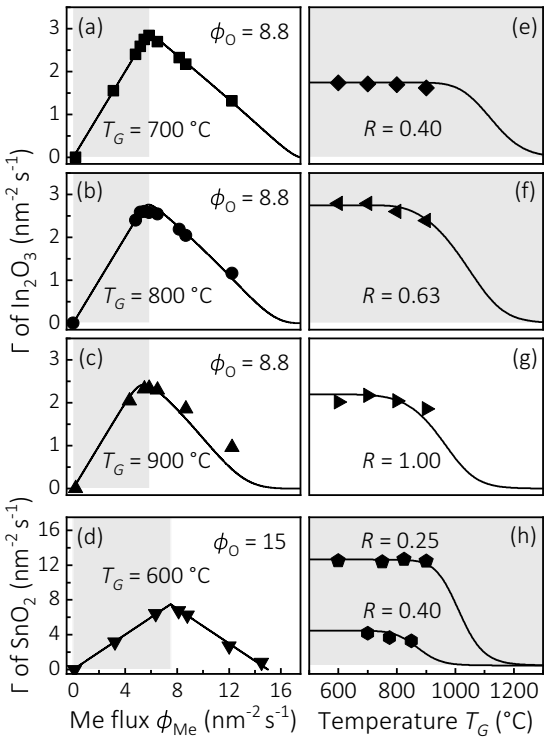

FIG. 2. (a)–(c) and (d) Dependence of Γ for In_2O_3 and SnO_2 on ϕ_{Me}, respectively, for different $T_G \pm 15$ °C and ϕ_O (in nm^{-2} s^{-1}), as indicated in the figures. [(e)–(g) and (h)] T_G dependence of Γ for In_2O_3 and SnO_2, respectively, at different $R \pm 0.02$, as indicated in the figures. Solid lines are model predictions by Eqs. (8) and (9), respectively, using Eqs. (10) and (11). Data in (h) for $R = 0.40$ were taken from Ref. [24], and the one for $R = 0.25$ are unpublished. Intersections with the Γ-axis account for the supplied $\phi_{Me} = x\Gamma$.

To microscopically explain our Γ and γ dependencies, we propose a general reaction scheme for III-O and IV-O compounds in Fig. 3. It depicts a Me_xO_y layer, impinging ϕ_{Me}, and ϕ_O, producing the Me (n_m), O (n_o), and suboxide (n_s) surface populations. The desorption of Me and O from the growth surface is characterized by desorption rate constants υ_m and υ_o, respectively. Two potential reactions to form Me_xO_{y-x} exist; (i) the direct oxidation of the Me to Me_xO_{y-x}—via a first oxidation step—through reaction

$$x\mathrm{Me}\,(a) + (y-x)\mathrm{O}\,(a) \xrightarrow{\upsilon_f} \mathrm{Me}_x\mathrm{O}_{y-x}\,(a), \qquad (1)$$

with suboxide formation rate constant υ_f, or (ii) via elemental Me etching of a Me_xO_y layer [21] through reaction

$$x(y-1)\mathrm{Me}\,(a) + \mathrm{Me}_x\mathrm{O}_y\,(s) \xrightarrow{\upsilon_e} y\mathrm{Me}_x\mathrm{O}_{y-x}\,(a), \qquad (2)$$

with etching rate constant υ_e. The adsorbate and solid phases are denoted as a and s, respectively. At elevated T_G, or in the Me-rich regime, the suboxide desorbs off the growth surface characterized by desorption rate constant υ_s. The Me_xO_{y-x} can be further oxidized to Me_xO_y—via a second oxidation step—through reaction

$$\mathrm{Me}_x\mathrm{O}_{y-x}\,(a) + x\mathrm{O}\,(a) \xrightarrow{\upsilon_g} \mathrm{Me}_x\mathrm{O}_y\,(s), \qquad (3)$$

with growth rate constant υ_g.

Our model (schematic in Fig. 3) is mathematically described by the set of coupled equations:

$$\dot{n}_m = \phi_{Me} - x\upsilon_f n_m^x n_o - x(y-1)\upsilon_e n_m^{x(y-1)} n_l - \upsilon_m n_m, \quad (4)$$

$$\dot{n}_o = \phi_O - \upsilon_f n_m^x n_o - x\upsilon_g n_s n_o^x - \upsilon_o n_o, \quad (5)$$

$$\dot{n}_s = \left(\upsilon_f n_m^x n_o + y\upsilon_e n_m^{x(y-1)} n_l\right) - \upsilon_g n_s n_o^x - \upsilon_s n_s. \quad (6)$$

In dynamic equilibrium, $\dot{n}_i \equiv \mathrm{d}n_i/\mathrm{d}t = 0$ (with i = m, o, s). The Me_xO_y surface population n_l as given in Eqs. (4) and (6) is determined by the layer. The second and third term in Eq. (4) account for Me_xO_{y-x} formation through reactions (1)

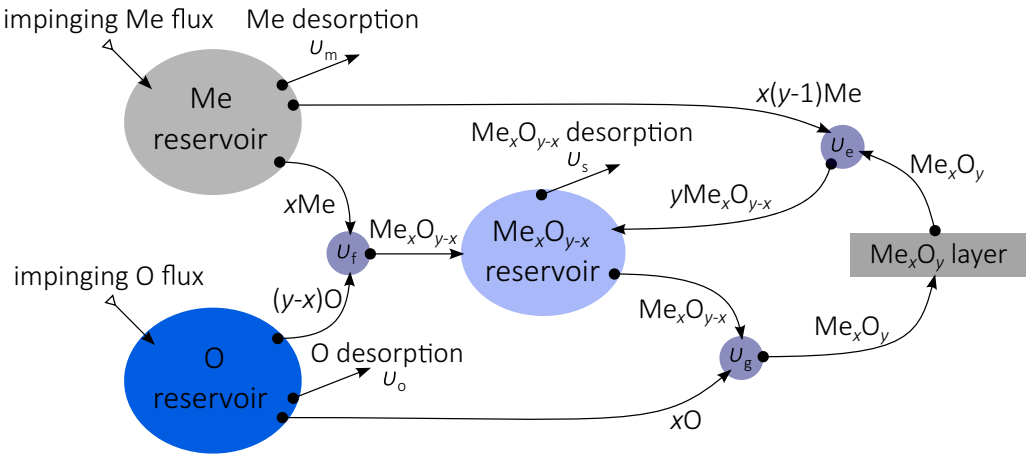

FIG. 3. Growth scheme for III-O and IV-O PAMBE showing impinging fluxes, resulting reservoirs, and a Me_xO_y layer. Possible chemical reactions and desorption rates occurring are indicated by respective rate constants υ_r ($r = \mathrm{m},\ \mathrm{o},\ \mathrm{f},\ \mathrm{s},\ \mathrm{g},\ \mathrm{e}$).

and (2), respectively. The Me, O, and Me_xO_{y-x} desorption rates are represented in the last terms of Eqs. (4), (5), and (6), respectively, and Γ is

$$\Gamma = \upsilon_g n_s n_o^x - \upsilon_e n_m^{x(y-1)} n_1. \tag{7}$$

We have never observed Me desorption for all growth conditions employed, hence, we assume that the Me-depleting process by suboxide formation is much faster than the one by Me desorption. Thus, we set $\upsilon_m \equiv 0$. To further reduce the complexity of our model, we assume that layer decomposition by reaction (2) is negligible, i.e., we set $\upsilon_e \equiv 0$, and consequently, $\upsilon_f \gg 0$. This assumption is reasonable since reaction (1) is kinetically preferred over reaction (2) because Me_xO_y needs to be formed first before being decomposed to Me_xO_{y-x}. These deductions are in agreement with the significantly higher vapor pressures of Me_xO_{y-x} compared to those of the Me, and additionally, to the Me_xO_y decomposition rates [23,25–28]. For the latter, we have not observed, e. g., a Ga_2O_3 decomposition at growth chamber pressures $p_{GC} \geqslant 10^{-8}$ Torr and $T_G \leqslant 1000\,^{\circ}$C by LR and QMS either (not shown). These p_{GC} and T_G are far below and above, respectively, the values where Ga_2O_3 thin film formation is possible (see Fig. 1)—further confirming our proposed two-step reaction mechanism. Moreover, our kinetic assumptions are supported thermodynamically showing that reaction (1) is energetically favored over reaction (2) [29]. Therefore we assume in our model, that all Me is oxidized via a *first* oxidation step to Me_xO_{y-x} through reaction (1), and the Me_xO_{y-x} can be further oxidized to Me_xO_y via a *second* oxidation step through reaction (3). This consecutive reaction mechanism is likely universal for all binary III-VI and IV-VI compounds as justified below and thermodynamically supported in Ref. [29].

Solving Eqs. (5) and (6) with respect to n_s and n_o, using Eq. (4) with $\upsilon_e = \upsilon_m \equiv 0$ and $\upsilon_f \gg 0$, and inserting the solutions in Eq. (7) yields Γ for III-VI materials (e.g., Ga_2O_3 and In_2O_3):

$$\Gamma = A^{-1}\left(\Upsilon - \tfrac{3}{4}\phi_{Me}^2 + \phi_{Me}\phi_O - \tfrac{1}{12}(2\phi_O - A)^2\right), \tag{8}$$

with function $A \equiv A(\Upsilon,\ \phi_{Me},\ \phi_O)$ given in Ref. [30]. For IV-VI materials (e.g., SnO_2), Γ simply reads as

$$\Gamma = \frac{1}{2}(\Upsilon + \phi_O - \sqrt{\Upsilon^2 + 2\Upsilon\phi_O + (2\phi_{Me} - \phi_O)^2}). \tag{9}$$

We note $\gamma = \phi_{Me} - \Gamma$, thus, our model describes all Me_xO_{y-x} desorption rates as well.

We factorized the residual rate constants υ_j ($j = \mathrm{s},\ \mathrm{o},\ \mathrm{g}$) to

$$\Upsilon(R, T_G) = \frac{\upsilon_s \upsilon_o}{\upsilon_g} = \prod_j \upsilon_0^j\, e^{\left(-\frac{e_a^j(R)}{k_B T_G}\right)} = \Upsilon_0\, e^{\left(-\frac{E_a(R)}{k_B T_G}\right)}, \tag{10}$$

with Boltzmann constant k_B. The individual pre-exponential factors and activation energies are υ_0^j and e_a^j, respectively. This approach further reduces the number of unknown kinetic model parameters from (originally) twelve to two, namely, $\Upsilon_0 = \prod_j \upsilon_0^j$ and $E_a = \sum_j e_a^j$. At this point, the complex reaction processes of III-O and IV-O compounds as illustrated in Fig. 3 have been collapsed to a simple quantitative model with only two parameters that can be fit to our experimental data.

The desorption of Me_xO_{y-x} is the only reduction channel of Γ, hence, we assume constant $\Upsilon_0 \approx \upsilon_0^s$ (given in Table I). The values of υ_0^s were obtained from literature by fitting the corresponding vapor pressure data of Me_xO_{y-x} [31–33], as well as by appropriate pressure to flux unit conversions. Consequently, the only remaining free parameter is E_a. Allowing the value of E_a to be freely adjustable, we performed least-square fits of Eq. (8) to the T_G dependence of Γ of Ga_2O_3 and In_2O_3, as well as of Eq. (9) to the one of SnO_2. The obtained values of E_a follow a linear dependence on R:

$$E_a(R) = E_0 - \varsigma R, \tag{11}$$

with $E_a(R = 0) = E_0$ and slope ς. All fit values are collected in Table I.

Equation (11) is used in Eq. (10), which, in turn, is inserted into Eqs. (8) and (9) for the corresponding III-O or IV-O compound, respectively. We propose this approach can be applied to other III-VI and IV-VI materials, as well.

Using the solutions obtained for Ga_2O_3, In_2O_3, and SnO_2 all Γ's can be modeled accurately as a function of all growth

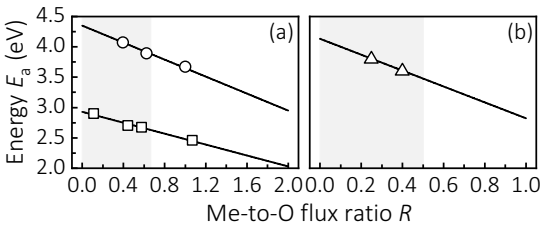

FIG. 4. (a) Activation energy E_a for Ga_2O (squares) and In_2O (discs) desorption from $Ga_2O_3(\bar{2}01)$ and $In_2O_3(111)$, respectively, as a function of $R \leqslant 2$. (b) Dependence of E_a on $R \leqslant 1$ for the desorption of SnO (triangles) from $SnO_2(101)$. Symbols represent experimental data obtained by fitting the T_G dependence of Γ as plotted in Figs. 1 and 2. The solid lines are linear fits of Eq. (11) to the data.

parameters, as drawn as solid lines in Figs. 1 and 2. Note that for the data shown, e.g., in Fig. 1(d), ϕ_O was three times larger than for the data depicted in Figs. 1(a)–1(c), illustrating our model desrcibes the complete PAMBE of III-VI and IV-VI compounds.

Equations (10) and (11) are in accordance with our experimental data showing an exponential increase of Me_xO_{y-x} desorption with increasing T_G *and* increasing R. We explain this behavior by a Me_xO_{y-x} surface coverage, θ, dependent kinetics of Me_xO_{y-x}. Moreover, we suppose first-order adsorption and desorption rates, thus, $\theta \propto n_s \propto \phi_{Me} \propto R \leqslant x$ [as indicated in Eqs. (4)–(6)]. We conclude that the fact of a decreasing E_a with R indicates repulsive interadsorbate interactions between Me_xO_{y-x}. This, in turn, results in an increased desorption rate of Me_xO_{y-x} at higher R and same T_G. We note that the value of $E_a(R)$ is growth system-dependent and material-specific—e.g., as indicated by a surface-orientation dependent Ga incorporation into Ga_2O_3 [34,35]—hence, can only be determined from experiment. $E_a(R)$ corresponds to the sum of the vertical adhesive energies between Me_xO_{y-x} and growth surface and lateral interactions of adsorbates (e.g., between Me_xO_{y-x} and O species). Our obtained ς reflects an alteration of these lateral adsorbate interactions depending on $\theta \propto R$. An increase of R leads to a change in the partition function of the adsorbed species [36,37]. Consequently, leads to a change in the surface energetics (e.g., the surface chemcial potential) of the corresponding III-VI or IV-VI growth system. θ-dependent adsorbate interactions have been described in many other material systems [37–42], and observed, e.g., for the desorption kinetics of In [43] and Ga [44] on an InN and GaN surface, respectively.

To conclude, we identified and quantitatively modeled the two-step reaction mechanism during III-O and IV-O PAMBE, via the intermediate formation of Me_xO_{y-x}. Based on this mechanism, the desorption of Me_xO_{y-x} was found to be the Γ-limiting step for these materials. These findings are fundamentally different, e.g., to the single-step reaction PAMBE of III-V semiconductors. Here, either Me desorption or layer decomposition [8] are the Γ-limiting processes. Moreover, the consistent quantitative description of all Γ's by our model, under a variety of growth conditions for III-O and IV-O materials with different stoichiometries, suggests the generality of our model for all III-O and IV-O compounds.

TABLE I. Collection of the model parameters Υ_0 as taken from literature, as well as E_0 and ς yielded by fitting the linear R-dependence, Eq. (11), of E_a as plotted in Fig. 4.

	Υ_0 ($nm^{-2}\,s^{-1}$)	E_0 (eV)	ς (eV)
Ga_2O_3	$e^{37.1}$ [31]	2.93 ± 0.03	0.45 ± 0.07
In_2O_3	$e^{37.3}$ [32]	4.35 ± 0.08	0.70 ± 0.25
SnO_2	$e^{37.7}$ [33]	4.13 ± 0.10	1.31 ± 0.04

The combination of the recently observed Me-exchange catalysis in oxide systems [45,46] with the present binary growth model provides a basis for the development of growth models describing the Me incorporation into ternary oxides [47,48] or complex oxide compounds [49,50]. Microscopic growth models would need to describe suboxides as surface adsorbed and diffusing species.

We conjecture our findings can be transferred to other epitaxial growth techniques such as pulsed laser deposition [51] and Me-organic vapor phase epitaxy [52], where similar kinetic effects are observed.

Finally, we predict a two-step reaction mechanism for other III-VI and IV-VI compounds whose kinetic and thermodynamic properties are comparable to those of the III-O and IV-O semiconductors presented in this Rapid Communication. For example, the III-Se, IV-Se, III-S, or III-Te compounds posses subselenides, subsulfurides, or subtellurides such as Ga_2Se [53], In_2Se [54,55], SnSe [56], In_2S [57], or In_2Te [58]. In fact, during the MBE of, e.g., Ga_2Se_3 [59] and In_2Se_3 [55], a similar Γ evolution, as for the III-O and IV-O semiconductors presented, has been observed: a decreasing Γ in the Me-rich regimes and a growth stop at high III/Se flux ratios. This behavior was attributed to the desorption of In_2Se in the case of In_2Se_3 MBE [55], for instance. Besides this experimental evidence, our calculations given in Ref. [29] also support the thermodynamic feasibility of the two-step growth mechanism for III-Se, IV-Se, III-Te, and III-S compounds. Therefore, we assume our model to be valid for a wide range of III-VI and IV-VI compounds.

We deeply acknowledge Oliver Brandt and Vladimir Kaganer for fruitful discussions regarding the growth model, Sergio Fernández-Garrido and Günter Wagner for a critical reading of the manuscript, as well as Hans-Peter Schönherr for technical MBE support. This work was performed in the framework of GraFOx, a Leibniz-Science Campus partially funded by the Leibniz association.

[1] S. Nakamura, Rev. Mod. Phys. **87**, 1139 (2015).
[2] H. Kroemer, Rev. Mod. Phys. **73**, 783 (2001).
[3] A. Y. Cho, J. Appl. Phys. **42**, 2074 (1971).
[4] H. Kroemer, Phys. Scr. **T68**, 10 (1996).
[5] K. Y. Cheng, J. Vac. Sci. Technol. **31**, 050814 (2013).
[6] K. Ploog, Annu. Rev. Mater. Sci. **11**, 171 (1981).
[7] K. Ploog, Annu. Rev. Mater. Sci. **12**, 123 (1982).
[8] S. Fernández-Garrido, G. Koblmüller, E. Calleja, and J. S. Speck, J. Appl. Phys. **104**, 033541 (2008).

[9] H. Kato, M. Sano, K. Miyamoto, and T. Yao, Jpn. J. Appl. Phys. **42**, 2241 (2003).

[10] Ü. Özgür, Y. I. Alivov, C. Liu, A. Teke, M. A. Reshchikov, S. Doğan, V. Avrutin, S.-J. Cho, and H. Morkoç, J. Appl. Phys. **98**, 041301 (2005).

[11] J. Ralston, G. W. Wicks, and L. F. Eastman, J. Vac. Sci. Technol. B **4**, 594 (1986).

[12] B. Heying, R. Averbeck, L. F. Chen, E. Haus, H. Riechert, and J. S. Speck, J. Appl. Phys. **88**, 1855 (2000).

[13] J. Neugebauer, T. K. Zywietz, M. Scheffler, J. E. Northrup, H. Chen, and R. M. Feenstra, Phys. Rev. Lett. **90**, 056101 (2003).

[14] G. Koblmüller, S. Fernández-Garrido, E. Calleja, and J. S. Speck, Appl. Phys. Lett. **91**, 161904 (2007).

[15] E. Calleja, M. A. Sánchez-García, F. J. Sánchez, F. Calle, F. B. Naranjo, E. Muñoz, S. I. Molina, A. M. Sánchez, F. J. Pacheco, and R. García, J. Cryst. Growth **201-202**, 296 (1999).

[16] M. Higashiwaki and G. H. Jessen, Appl. Phys. Lett. **112**, 060401 (2018).

[17] O. Bierwagen, Semicond. Sci. Technol. **30**, 024001 (2015).

[18] O. Bierwagen, T. Nagata, M. E. White, M.-Y. Tsai, and J. S. Speck, J. Mater. Res. **27**, 2232 (2012).

[19] M.-Y. Tsai, M. E. White, and J. S. Speck, J. Appl. Phys. **106**, 024911 (2009).

[20] M.-Y. Tsai, O. Bierwagen, M. E. White, and J. S. Speck, J. Vac. Sci. Technol. A **28**, 354 (2010).

[21] P. Vogt and O. Bierwagen, Appl. Phys. Lett. **106**, 081910 (2015).

[22] P. Vogt and O. Bierwagen, Appl. Phys. Lett. **108**, 072101 (2016).

[23] P. Vogt and O. Bierwagen, Appl. Phys. Lett. **109**, 062103 (2016).

[24] M. E. White, M.-Y. Tsai, F. Wu, and J. S. Speck, J. Vac. Sci. Technol. A **26**, 1300 (2008).

[25] J. H. Lamoreaux, V. A. Borjakova, and V. F. Shevelkov, J. Phys. Chem. Ref. Data **16**, 419 (1987).

[26] Z. Galazka, R. Uecker, K. Irmscher, M. Albrecht, D. Klimm, M. Pietsch, M. Brützam, R. Bertram, S. Ganschow, and R. Fornari, Cryst. Res. Technol. **45**, 1229 (2010).

[27] Z. Galazka, R. Uecker, K. Irmscher, D. Schulz, D. Klimm, M. Albrecht, M. Pietsch, S. Ganschow, A. Kwasniewski, and R. Fornari, J. Cryst. Growth **362**, 349 (2013).

[28] Z. Galazka, R. Uecker, D. Klimm, K. Irmscher, M. Pietsch, R. Schewski, M. Albrecht, A. Kwasniewski, S. Ganschow, D. Schulz, C. Guguschev, R. Bertram, M. Bickermann, and R. Fornari, Phys. Status Solidi A **211**, 66 (2014).

[29] See Supplemental Material at http://link.aps.org/supplemental/10.1103/PhysRevMaterials.2.120401 for thermochemical calculations of Eqs. (1)–(3) for various III-VI and IV-VI compounds as well as a detailed description of Eq. (11).

[30] The function $A \equiv A(\Upsilon,\ \phi_{\mathrm{Me}},\ \phi_{\mathrm{O}})$ included in Eq. (8) explicitly reads as

$$A = [72\Upsilon\phi_{\mathrm{O}} - (3\phi_{\mathrm{Me}} - 2\phi_{\mathrm{O}})^3 + \sqrt{108}\{\Upsilon[16\Upsilon^2 - 4\Upsilon(9\phi_{\mathrm{Me}}^2 - 12\phi_{\mathrm{Me}}\phi_{\mathrm{O}} - 8\phi_{\mathrm{O}}) + (\phi_{\mathrm{Me}} - 2\phi_{\mathrm{O}})(3\phi_{\mathrm{Me}} - 2\phi_{\mathrm{O}})^3]\}^{\frac{1}{2}}]^{\frac{1}{3}},$$

with Υ being a function of T_G, as explicitly given in Eq. (10).

[31] C.-J. Frosch and C.-D. Thurmond, J. Phys. Chem. **66**, 877 (1962).

[32] J. Valderrama-N and K.-T. Jacob, Thermochim. Acta **21**, 215 (1977).

[33] R. Colin, J. Drowart, and G. Verhaegen, Trans. Faraday Soc. **61**, 1364 (1965).

[34] K. Sasaki, A. Kurumata, T. Masui, E. G. Víllora, K. Shimamura, and S. Yamakoshi, Appl. Phys. Express **5**, 035502 (2012).

[35] Y. Oshima, E. Ahmadi, S. Kaun, F. Wu, and J. S. Speck, Semicond. Sci. Technol. **33**, 015013 (2017).

[36] J. K. Garbacz and M. Jaroniec, Thin Solid FIlms **100**, 43 (1983).

[37] K. A. Peterlinz, T. J. Curtiss, and S. J. Sibener, J. Chem. Phys. **95**, 6972 (1991).

[38] H. Pfnür and D. Menzel, J. Chem. Phys. **79**, 2400 (1983).

[39] H. Pfnür, P. Feulner, and D. Menzel, J. Chem. Phys. **79**, 4613 (1983).

[40] I. G. Pitt, R. G. Gilbert, and K. R. Ryan, J. Chem. Phys. **102**, 3461 (1995).

[41] C. Stampfl, H. J. Kreuzer, S. H. Payne, H. Pfnür, and M. Scheffler, Phys. Rev. Lett. **83**, 2993 (1999).

[42] V. P. Zhdanov, J. Chem. Phys. **114**, 4746 (2001).

[43] G. Koblmüller, C. S. Gallinat, and J. S. Speck, J. Appl. Phys. **101**, 083516 (2007).

[44] L. He, Y. T. Moon, J. Xie, M. Muñoz, D. Johnstone, and H. Morkoç, Appl. Phys. Lett. **88**, 071901 (2006).

[45] P. Vogt, O. Brandt, H. Riechert, J. Lähnemann, and O. Bierwagen, Phys. Rev. Lett. **119**, 196001 (2017).

[46] P. Vogt, A. Mauze, F. Wu, B. Bonef, and J. S. Speck, Appl. Phys. Express **11**, 115503 (2018).

[47] P. Vogt and O. Bierwagen, APL Mater. **4**, 086112 (2016).

[48] Y. Oshima, E. Ahmadi, S. C. Badescu, F. Wu, and J. S. Speck, Appl. Phys. Express **9**, 061102 (2016).

[49] D. G. Schlom, APL Mater. **3**, 062403 (2015).

[50] S. Raghavan, T. Schumann, H. Kim, J. Y. Zhang, T. A. Cain, and S. Stemmer, APL Mater. **4**, 016106 (2016).

[51] S. Müller, H. v. Wenckstern, D. Splith, F. Schmidt, and M. Grundmann, Phys. Status Solidi A **211**, 34 (2014).

[52] G. Wagner, M. Baldini, D. Gogova, M. Schmidbauer, R. Schewski, M. Albrecht, Z. Galazka, D. Klimm, and R. Fornari, Phys. Status Solidi A **211**, 27 (2014).

[53] D. G. A. Gamal, A. T. Nagat, M. M. Nassary, and A. M. Abou-Alwafa, Cryst. Res. Technol. **31**, 359 (1996).

[54] J. H. Greenbergl, V. A. Borjakova, and V. F. Shevelkov, J. Chem. Thermodyn. **5**, 233 (1973).

[55] T. Okamoto, A. Yamada, and M. Konagai, J. Cryst. Growth **175-176**, 1045 (1997).

[56] V. P. Bhatt, K. Gireesan, and G. R. Pandya, J. Cryst. Growth **96**, 649 (1989).

[57] P. Mukdeeprom and J. G. Edwards, Thermochim. Acta **112**, 141 (1987).

[58] T. D. Golding, P. R. Boyd, M. Martinka, P. M. Amirtharaj, J. H. Dinan, S. B. Qadri, D. R. T. Zahn, and C. R. Whitehouse, J. Appl. Phys. **65**, 1936 (1989).

[59] N. Teraguchi, F. Kato, M. Konagai, K. Takahashi, Y. Nakamura, and N. Otsuka, Appl. Phys. Lett. **59**, 567 (1991).

Correction: The originally published Figure 3 contained a resolution error and has been fixed. Inconsistencies in figure regime identifications have been fixed. Missing error values for some quantities have been inserted. Equation (10) and the first line in Table I, last column, contained minor errors and have been fixed.